OPEN ACCESS

Condensed Matter Physics ARTICLE

The Innovation Physics

Anomalous ferroic transitions deviating from the model of Landau theory

Yuxuan Sheng[1] **and Menghao Wu**[1,*]

*Correspondence: wmh1987@hust.edu.cn

Received: April 27, 2026; Accepted: September 9, 2026; Published Online: September 9, 2026; https://doi.org/10.59717/j.tip.2026.100017

© 2026 The Author(s). This is an open access article under the CC BY license (https://creativecommons.org/licenses/by/4.0/).

GRAPHICAL ABSTRACT

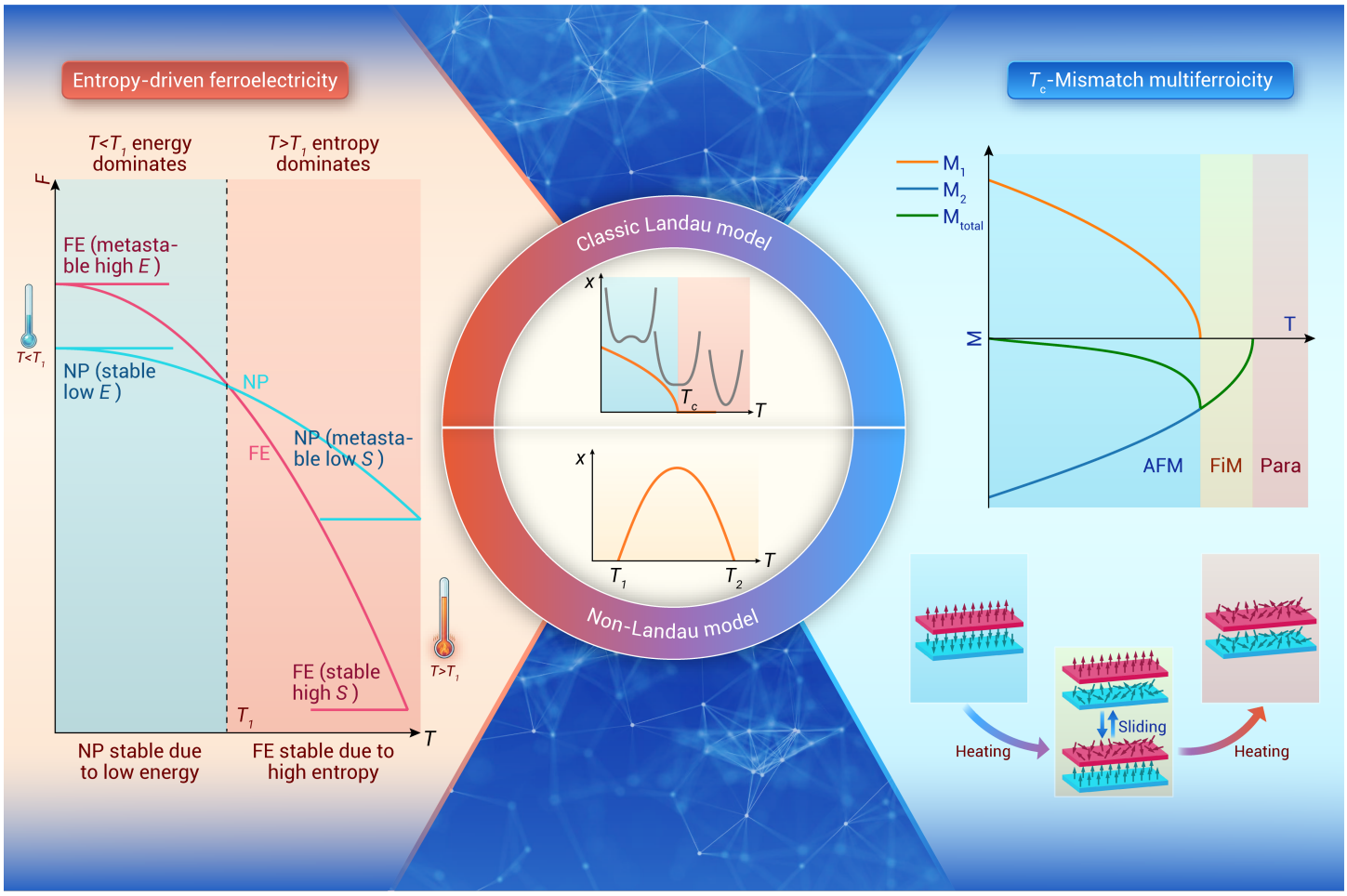

PUBLIC SUMMARY

- We predict anomalous phase transitions where ferroic orders peak at elevated temperatures.
- Such behaviors may emerge in some unconventional ferroelectrics with long ion displacements.
- They also occur in some compensated antiferromagnets, which may lead to unconventional strong multiferroicity.

ARTICLE Condensed Matter Physics

OPEN ACCESS

Anomalous ferroic transitions deviating from the model of Landau theory

Yuxuan Sheng[1] **and Menghao Wu**[1,*]

[1]School of Physics and School of Chemistry, Institute of Theoretical Chemistry, Huazhong University of Science and Technology, Wuhan 430074, China

*Correspondence: wmh1987@hust.edu.cn

Received: April 27, 2026; Accepted: September 9, 2026; Published Online: September 9, 2026; https://doi.org/10.59717/j.tip.2026.100017

© 2026 The Author(s). This is an open access article under the CC BY license (https://creativecommons.org/licenses/by/4.0/).

Citation: Sheng Y. and Wu M. (2026). Anomalous ferroic transitions deviating from the model of Landau theory. *The Innovation Physics* **1**:100017.

Landau theory has been an effective model to describe ferroelectric and ferromagnetic transitions over the past century, where the polarization and magnetization decrease with temperature and disappear above the Curie temperature. In this paper we predict an anomalous temperature dependence of polarization or magnetization with maxima located at elevated temperatures, contrary to classical model. One class of examples may exist in emerging ferroelectrics with long ion displacements and quantized polarizations. Their ferroelectric switching pathways involve non-polar stable phases with low entropy, which become more favorable in free energy at low temperatures compared with polar phases. Another class includes Luttinger-compensated antiferromagnets with non-relativistic spin splittings, composed of two opposite spin sublattices with different spin exchange constants and thus different Curie temperature. Such a difference can be utilized to generate a unique type of multiferroicity, where large magnetizations can be reversed via ferroelectric switching between two Curie temperature with alternating half of spins in paramagnetic state. We demonstrate these proposals by first-principles calculations assisted by machine-learning-based force fields and Monte Carlo simulations, based on several paradigmatic systems composed of synthesized intercalated ferroelectric/magnetic materials. Our proposed new models may greatly broaden the scope of ferroicity/multiferroicity and help explain some previously unclarified phenomena.

INTRODUCTION

Ferroic materials are characterized by the presence of a spontaneous and switchable order parameter arising from spontaneous symmetry breaking below the Curie temperature (T_c), such as polarization in ferroelectrics and magnetization in ferromagnets. The ferroic phase transition can be described by Landau theory based on an expansion of the free energy F of a thermodynamic system[1] in terms of an order parameter χ:

$$F(T) = F_0 + \frac{1}{2}\alpha(T - T_c)\chi^2 + \frac{1}{4}\beta\chi^4$$

where $\beta > 0$ ensures stability. When $T < T_c$, such formula give rises to a typical double-well potential for bi-stable states. The equilibrium configuration is determined by the minima of F:

$$\frac{\partial F}{\partial \chi} = \alpha(T - T_c)\chi + \beta\chi^3 = 0$$

$$\chi = \begin{cases} 0, & T > T_c \\ \pm\sqrt{\dfrac{\alpha(T_c - T)}{\beta}}, & T < T_c \end{cases}$$

indicating a continuous emergence of long-range ferroic order through a second-order phase transition as thermal fluctuations subside. As the temperature rises and exceeds T_c, $\alpha(T_c - T)$ becomes negative, driving the order parameter to zero and leading to the emergence of the disordered paraphase. Such Landau phenomenological model has been successfully applied to various ferroic systems in the past century, also including emerging new types like sliding ferroelectricity,[2,3] altermagnetism[4] and autferroicity.[5]

In this paper, we predict several cases that deviate from the classical model of ferroic transitions, where the ferroelectric polarization or magnetization diminishes at 0K while reaching a maximum at elevated temperature. Compared with typical ferroelectricity with small ion displacements from the paraelectric phase as transition state, some unconventional properties of ferroelectricity with long ion displacements have been explored recently. Their ferroelectric switching may involve ion migrations over multiple or fractional lattice constants, giving rise to quantized[6,7] or fractional quantum ferroelectricity,[8] and such ferroelectricity may even exist in non-polar crystals.[9] Here we propose that the phase transitions in such ferroelectricity may deviate from the model based on Landau theory since the large quantized polarizations cannot serve as a small expansion parameter. A similar anomalous temperature dependence also emerges in many magnetic systems including Luttinger compensated antiferromagnets, which become uncompensated at elevated temperature due to two spin sublattices with different exchange constants. We further show first-principles evidence that the uncompensated magnetization can be reversed via ferroelectric switching in some two-dimensional intercalated systems. Such electrically switchable magnetization can be unprecedentedly large—a property long-sought but elusive in previous multiferroics due to the mutual exclusivity between the two ferroic orders. It is noteworthy that type-I multiferroics mostly exhibit negligible magnetoelectric couplings, while type-II multiferroics possess much weaker polarizations and magnetizations.[10,11]

MATERIALS AND METHODS

Our first-principles calculations are performed based on the density functional theory (DFT) method implemented in Vienna Ab initio Simulation Packages (VASP 5.4.4) code.[29,30] The exchange–correlation effect described within the generalized gradient approximation in the Perdew–Burke–Ernzerhof[31] functional, together with the projector augmented wave[32] method, are adopted. GGA+$U_{effective}$[30] approach is used to deal with localized d orbitals, with U=5.67 eV for Cr in $Ag(CrS_2)_2$, 1.2 eV for the V in VSe_2, same as in previous studies.[20,24] The van der Waals correction of Grimme with Becke-Johnson damping function[33] is adopted and a 40 Å vacuum space is set to avoid the artificial interaction induced by period boundary conditions for all the layers. Brillouin zone integration is performed using 11 × 11 × 1 and 5 × 5 × 1 Monkhorst–Pack k-grids[34] respectively for the structure optimization and energy calculation of $AgCr_2S_4$, (lattice constant |a|=3.50 Å) and molecules

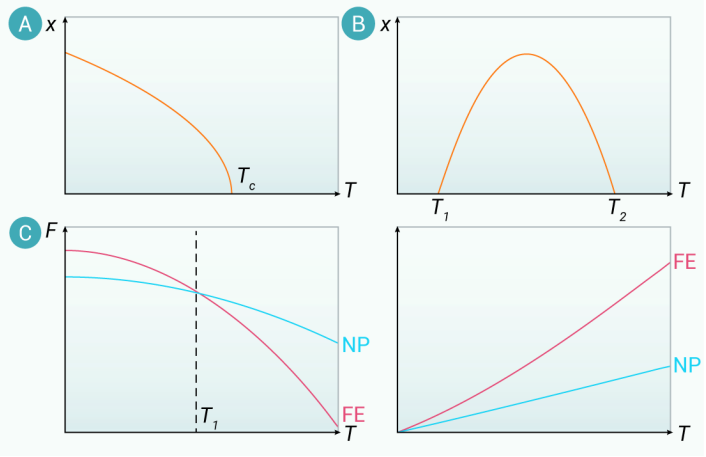

Figure 1. Model of anomalous ferroic transition Comparison between (A) Landau theory description of ferroic transition and (B) our predicted anomalous temperature dependence. (C) The temperature dependence of entropy and free energy for ferroelectric (FE) and non-polar (NP) phase in entropy-driven ferroelectric transition, where FE phase is slightly higher in energy and entropy compared with NP phase, and FE phase will become more favorable in free energy above critical temperature.

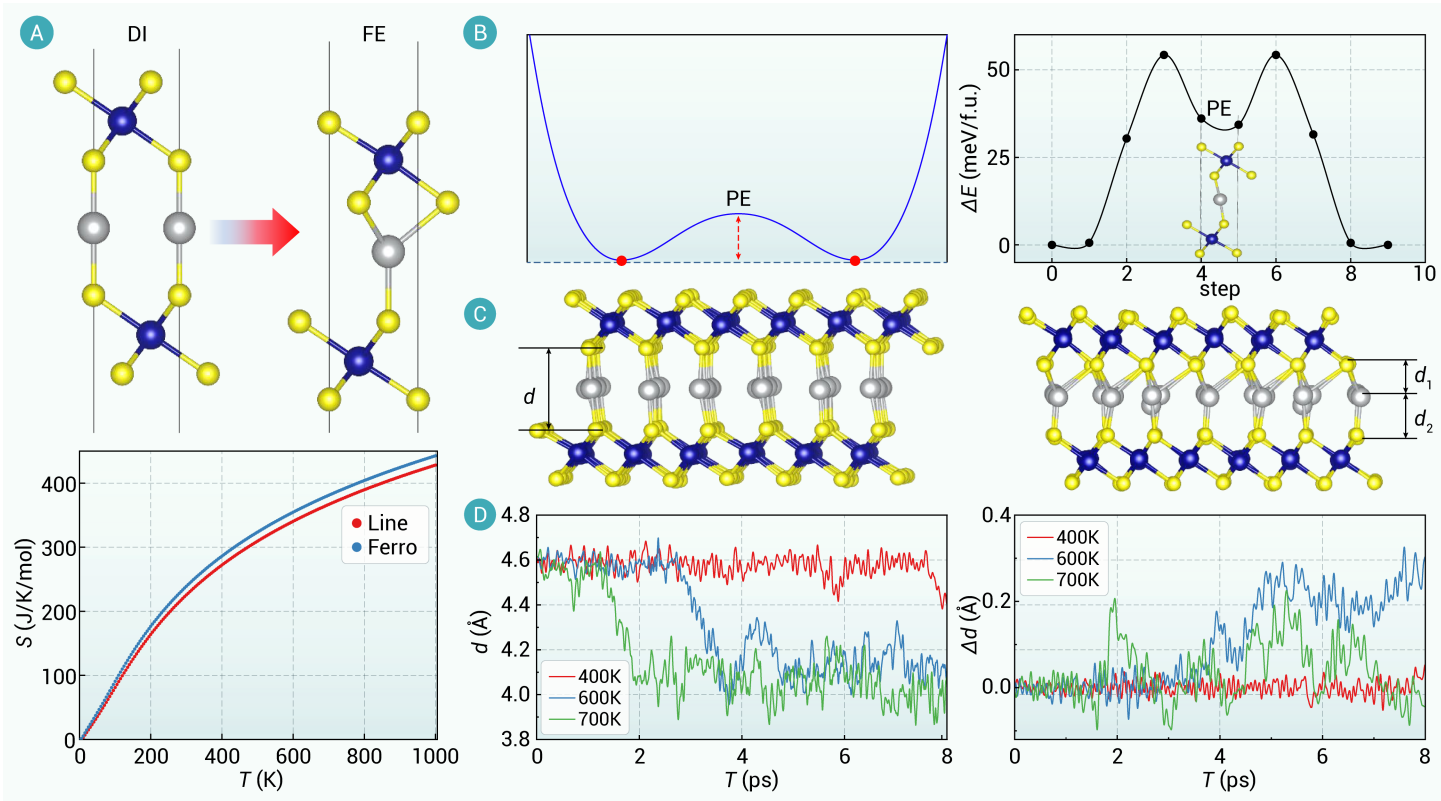

Figure 2. DI-FE phase transition of $AgCr_2S_4$ (A) DI and FE phase of $AgCr_2S_4$, and comparison of their entropy. (B) Double-well potential of classical ferroelectricity with PE state as a transition state, compared with the switching pathway of $AgCr_2S_4$ with PE state as a metastable state. (C) Snapshots of the equilibrium structures for $AgCr_2S_4$ at 400K and 600K at the end of 8 ps in AIMD simulations, and (D) corresponding evolution of interlayer distance d and Ag ion displacement $\Delta d=d_1-d_2$.

intercalated bilayers (|a|=13.71 Å for both systems). All the structures are fully relaxed until the energy and forces converged to 10^{-6} eV and 0.01 eV·Å^{-1}, respectively, where the kinetic energy cutoff is set to be 500 eV. The solid state nudged-elastic-band[35] (SS-NEB) method and Berry phase method[36] are respectively used for calculating the ferroelectric switching pathways and polarizations.

The software package DeePMD-kit[37,38] are adopted for training the machine learning force field. The DFT based AIMD calculations with gamma-only k points were performed for training data based on VASP 5.4.4, as mentioned above, where the timestep is set as 1.5 fs in the canonical ensemble. The training dataset consists of 74 000 frames under temperature series from 100 to 900 K with 100 K each steps, two extra 470 and 750 K were included, where 331 supercell is used. The cut-off radius is 6 Å along with the smoothing parameter of 0.5 Å. The starting learning rate is 10^{-3} and end with 10^{-8}. At the inference step, the LAMMPS[39] for NVT DPMD simulations are performed in 661 supercell.

RESULTS

First, we propose a possible mechanism that may induce such an atypical transition in ferroelectricity. The ferroelectric switching pathway of long ion displacements may involve various metastable phases, e.g., $CuCrX_2$ (X=S, Se) with Cu ions in sixfold coordination as the metastable paraelectric phase, which is slightly higher in energy compared with the ferroelectric ground state with Cu ions in fourfold coordination.[12] The ferroelectricity of $CuCrX_2$ has been experimentally confirmed in a series of reports,[13-15] including both conventional out-of-plane ferroelectricity and anomalous in-plane ferroelectricity violating Neumann's principle, and similar ferroelectricity has also been detected in thin-layer $AgCrS_2$.[16,17]

The anomalous behavior may take place if the polar phase possesses higher entropy S compared with the non-polar phase that is slightly lower in energy E, so that the polar phase with lower $F=E-TS$ will dominate above the critical temperature, as shown in Figure 1B. Herein $CuCrX_2$ is not a candidate since its ferroelectric phase is the ground state. However, in monolayer $AgCrS_2$ (or bilayer CrS_2 intercalated with Ag, i.e., $AgCr_2S_4$)[18,19] the Ag ions are inclined to form into non-polar di-coordinate configurations (denoted as the DI phase),[20] while the ferroelectric tetra-coordinate configurations (denoted as the FE phase) is slightly higher in both energy and entropy (Figure 2A). In this case, the FE phase becomes more favorable in free energy F=U-TS above around 220 K, as shown in Figure S1. Herein, the configurational entropy is ignored and only the vibration entropy obtained from the phonon dispersion is considered. However, it is plausible for the FE state to possess a larger entropy since its Ag-S bond length of around 2.67 Å is much longer than that of 2.37 Å in the DI state, indicating a more loosely bonded configuration.

Compared with the ground state DI phase, the FE phase possesses a smaller interlayer distance d and its intercalated Ag layer is vertically displaced from the midplane. Also distinct from the typical double-well model with a transition state as the paraelectric (PE) state, as shown in Figure 2B, in the ferroelectric switching pathway where Ag ions are displaced horizontally by 1/3 of a lattice constant, the PE state is metastable; thus, the soft modes vital to the formation of conventional ferroelectricity are absent here. Our *ab initio* molecular dynamics (AIMD) simulations in Figure 2C indicate that the phase transition occurs between 400 and 600K, also evidenced by the evolution of the average interlayer distance d in Figure 2D, which drastically shrinks from ~4.6 Å at 400 K to ~4.0 Å at 600 K and 700 K. The average vertical displacement of Ag ions $\Delta d=d_1-d_2$ (marked in Figure 2C) also increases to above 0.4 Å at 600 K from close to zero at 400 K, and falls back to approximately zero at 700 K, revealing the occurrence of a paraelectric-ferroelectric-paraelectric transition. Although the antiferroelectric state with a reduced distance between adjacent Ag ions is unstable due to the interionic repulsion between them, as shown in Figure S2, a disordered Ag-ion configuration can likely form at high temperature.

A machine-learning-based force field was further used for large-scale deep potential molecular dynamics (DPMD) simulations of the phase transition. The trained machine-learning potential field for calculating the force and energy reaches to approach the accuracy of AIMD, as shown in Figure 3A, where the root mean square errors (RMSEs) for the force and energy are respectively estimated to be ~0.046 eV/Å and ~1.13 meV/atom, respectively,

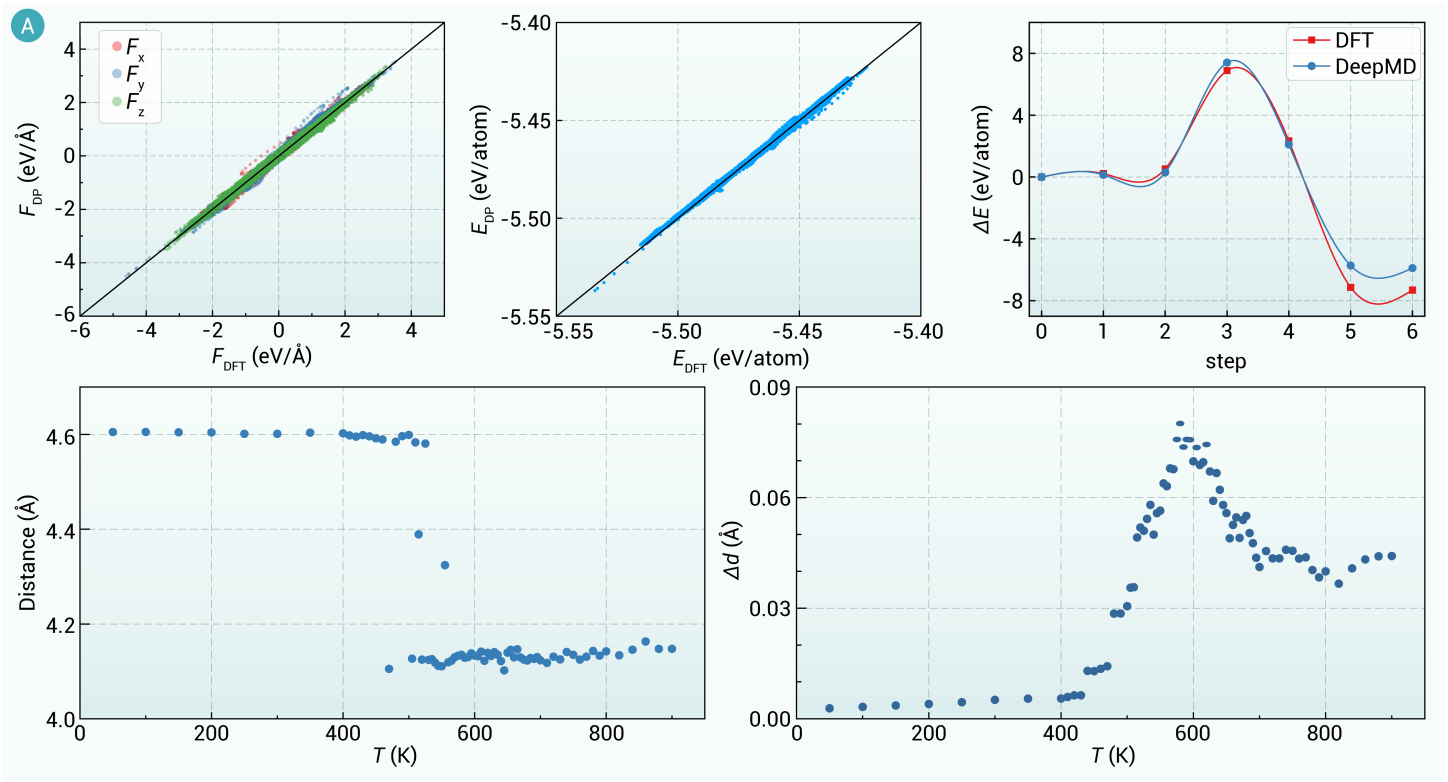

Figure 3. Deep potential molecular dynamics simulations of $AgCr_2S_4$ Comparison of (A) atomic forces, energies and (B) FE-DI transition pathway of $AgCr_2S_4$ calculated by DP model and DFT. (C) The temperature dependence of interlayer distance d and Ag ion displacement $\Delta d=d_1-d_2$.

after systematic training, and the energy evolution for the FE-DI transition is also well reproduced in Figure 3B. Herein a 252-atom supercell was adopted in the DPMD simulations for a 120 ps relaxation at each given temperature, where a step-like drastic decline in the average interlayer distance d is observed at ~470 K, indicating the occurrence of the DI-FE phase transition. The average vertical displacement of Ag ions $\Delta d=d_1-d_2$, which is closely related to the macroscopic polarization, also increases from close to zero at ~420 K, to its maximum at ~580 K.

We further propose another possible mechanism that may induce a similar transition. Suppose there is a ferrimagnetic system composed of two opposite spin sublattices, with distinct spin exchange constants that lead to distinct Curie temperatures T_1 and T_2 ($T_2 > T_1$), as shown in Figure 4A. If the coupling between them is negligible, according to the Landau theory, the net magnetization of the two layers $M=M_1+M_2$, may increase with T when $T<T_1$. In particular, this can be applicable to compensated antiferromagnets (sometimes denoted as Luttinger compensated magnets), which may become uncompensated at elevated temperatures, especially when one of the spin sublattices becomes paramagnetic leaving the other ferromagnetic, and this principle is similar to the so-called irreducible ferrielectricity proposed in a previous study.[21]

The potential candidates include various magnetic bilayer sliding ferroelectrics where the interlayer coupling is antiferromagnetic and the intralayer coupling is ferromagnetic.[22,23] The Curie temperatures of the top and bottom layers can be slightly different due to the interlayer inequivalence induced by vertical polarization. A similar difference in Curie temperatures induced by electric polarization may also emerge when a homobilayer ferromagnet is separated by a ferroelectric monolayer that also induces antiferromagnetic interlayer coupling, as illustrated in Figure 4B: the bilayer system with one ferromagnetic layer and the other close to the paraelectric phase between T_1 and T_2 exhibits a nonzero magnetization, which can be reversed upon ferroelectric switching due to the swapping of Curie temperatures between two layers.

Such atypical temperature-driven multiferroic coupling may yield a much larger switchable magnetization compared with that in either type-I or type-II multiferroics reported previously. Here we select a paradigmatic case based

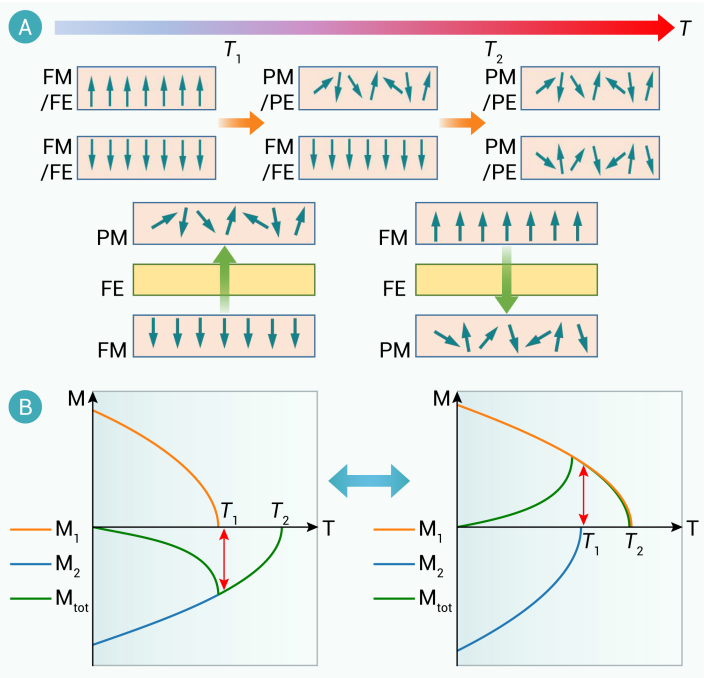

Figure 4. Model of anomalous temperature dependence in compensated antiferromagnets/antiferroelectrics and multiferroic hetero-trilayers (A) Evolution of two ferromagnetic (FM) or ferroelectric (FE) layers/lattices with different Curie temperature and opposite directions, where the compensated magnetization or polarization at 0K becomes uncompensated as only one of them become paramagnetic (PM) or paraelectric (PE) between two Curie temperature. (B) A sketch of temperature-driven multiferroicity: when the difference in Curie temperature between the top and bottom layer is induced by polarization of ferroelectric (FE) middle layer, a considerable uncompensated magnetization $M_{tot}=M_1+M_2$ marked by red arrow can be formed, which can be reversed via ferroelectric switching. The spin and polarization directions are respectively marked by olive and green arrows.

on previous studies:[24,25] when magnetic bilayers (e.g., VSe_2, CrI_3) are intercalated with molecules like titanium porphyrin (TiP) or vanadium porphyrin (VP),

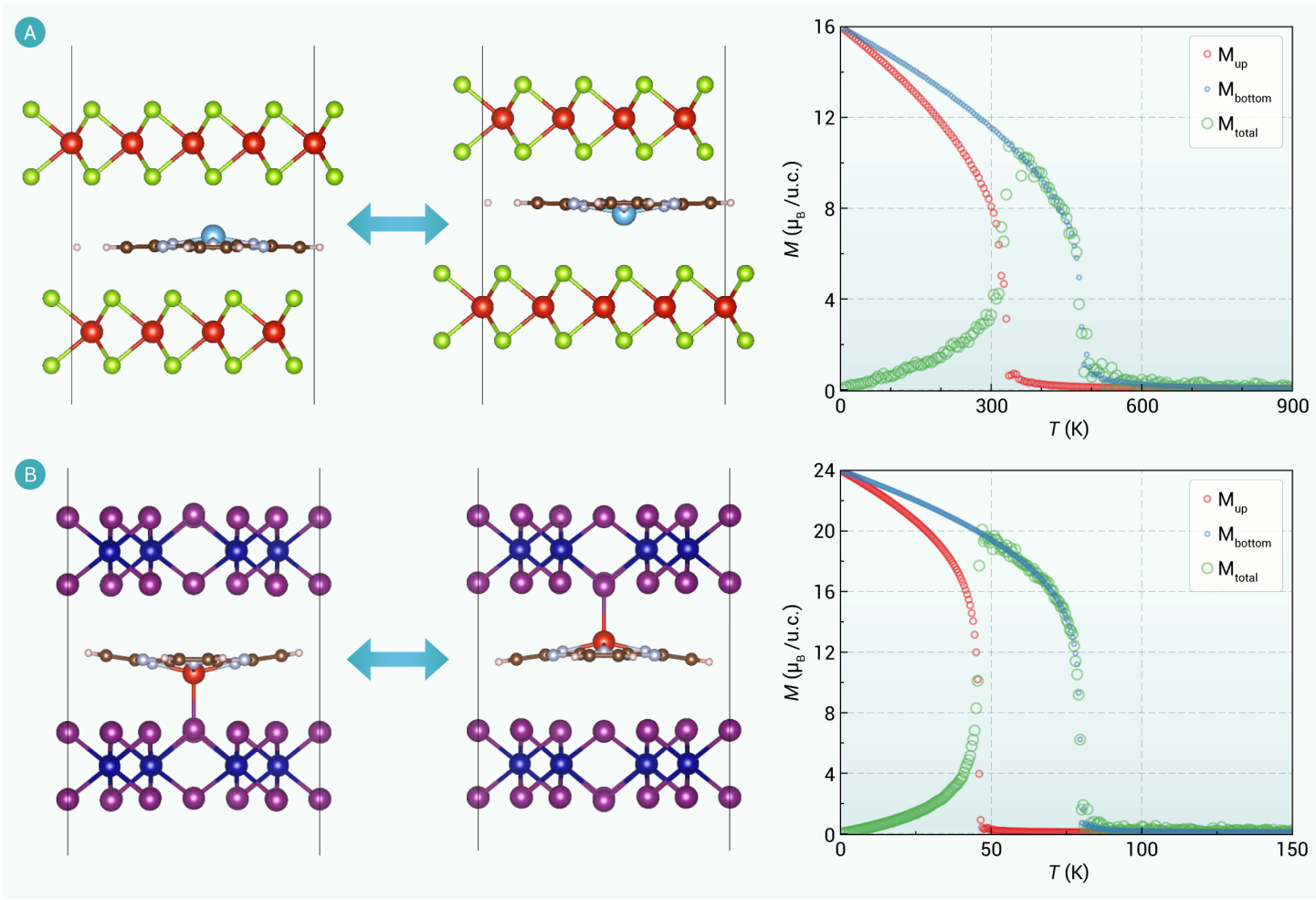

Figure 5. Large electrically switchable magnetizations in intercalated magnetic bilayers Ferroelectric switching between bi-stable polar states and temperature dependence of magnetization for (A) bilayer VSe_2 intercalated by TiP molecules and (B) bilayer CrI_3 intercalated by VP molecules. The magnetizations per unitcell (u.c.) of upper layer, bottom layer and the whole bilayer are respectively marked by red, blue, and green dot lines.

each metal ion is inclined to form a bond with one of the two layers, which gives rise to a vertical polarization switchable upon the sliding of molecules and vertical displacements of the metal ions. In such a bilayer with intralayer ferromagnetism and interlayer antiferromagnetic coupling, a considerable difference in the Curie temperatures of the two layers can be induced by the vertical polarization. Our predictions can be verified by Monte Carlo simulations based on Heisenberg model:

$$\hat{H} = -\frac{1}{2}\sum_{\langle ij \rangle} J\vec{S}_i \cdot \vec{S}_j - \sum_{\langle i \rangle} D(S_{iz})^2$$

where J is defined as the nearest-neighbor exchange coupling parameter, D (estimated to be 2.16 and 1.20 meV for monolayer VSe_2 and CrI_3) is the single-site magnetic anisotropy energy, and |S|=1/2 and 3/2 for monolayer VSe_2 and CrI_3, respectively. The calculated J values for the VSe_2 layer binding with TiP molecules and pristine VSe_2 monolayer are 160.63 meV and 109.38 meV, respectively. Such a difference is also notable in the CrI_3 layer binding with VP molecules and pristine CrI_3 with J estimated to be 5.6 and 2.8 meV, respectively. Due to the large interlayer difference in magnetic exchange parameters for intercalated bilayer VSe_2 and CrI_3, together with negligible interlayer coupling, a large switchable net magnetization is formed, reaching the maximum values of 10.74 and 19.95 μ_B, respectively, per unitcell (containing 32 V ions and 16 Cr ions, respectively) at $T = T_1$, as shown in Figures 5A-B.

CONCLUSION

In summary, we predict several anomalous cases where the polarization or magnetization increases with temperature from zero to a maximum. For unconventional ferroelectricity with long ion displacements, the large quantized polarization cannot serve as a small parameter in the Landau free-energy expansion. The switching pathway of long ion displacements may involve various metastable phases, which is also distinct from the long-established double-well potential model and soft mode model. This atypical behavior may emerge if the polar phase is higher both in energy and entropy compared with the non-polar phase, which may also explain some intriguing phenomena in organic ferroics.[26-28]

A similar anomalous behavior may also take place in compensated antiferromagnets with two opposite spin sublattices of different spin exchange parameters. Such a difference stems from polarization in some multiferroic systems, where ferroelectric switching swaps the paramagnetic state and ferromagnetic state between the two opposite spin lattices and reverses a large magnetization, which is distinct from the multiferroic coupling in previous studies. We demonstrate these proposals via first-principles calculations assisted by machine-learning-based force fields and Monte Carlo simulations on several paradigmatic systems, including magnetic bilayers intercalated with Ag ions or metal phophyrin molecules. Our predictions, which contrast conventional viewpoints, not only broaden the scope of ferroic transitions, but may also provide vast opportunities for revolutionizing the design of high temperature multiferroic memories devices.

REFERENCES

1. Levanyuk A. P., Burc Misirlioglu I. and Baris Okatan M. (2020). Landau, Ginzburg, Devonshire and others. *Ferroelectrics* **569**:310–323. DOI:10.1080/00150193.2020.1822684
2. Tang P. and Bauer G. E. W. (2023). Sliding phase transition in ferroelectric van der Waals bilayers. *Phys. Rev. Lett.* **130**:176801. DOI:10.1103/PhysRevLett.130.176801
3. Liu Y., Liu S., Li B., et al. (2022). Identifying the transition order in an artificial ferroelectric van der Waals heterostructure. *Nano Lett.* **22**:1265–1269. DOI:10.1021/acs.nanolett.1c04467

4. McClarty P. A. and Rau J. G. (2024). Landau theory of altermagnetism. *Phys. Rev. Lett.* **132**:176702. DOI:10.1103/PhysRevLett.132.176702
5. Zhang J. J., Yakobson B. I. and Dong S. (2025). Landau theory description of autferroicity. *Phys. Rev. Lett.* **134**:216801. DOI:10.1103/PhysRevLett.134.216801
6. Wu M., Burton J. D., Tsymbal E. Y., et al. (2013). Hydroxyl-decorated graphene systems as candidates for organic metal-free ferroelectrics, multiferroics, and high-performance proton battery cathode materials. *Phys. Rev. B* **87**:081406. DOI:10.1103/PhysRevB.87.081406
7. Wang X., Ren Y. and Wu M. (2022). Unconventional ferroelectricity with quantized polarizations in ionic conductors: High-throughput screening. *J. Phys. Chem. Lett.* **13**:9552–9557. DOI:10.1021/acs.jpclett.2c02601
8. Ji J., Yu G., Xu C., et al. (2024). Fractional quantum ferroelectricity. *Nat. Commun.* **15**:135. DOI:10.1038/s41467-023-44453-y
9. Sheng Y., Wu M. and Liu J. M. (2024). Ferroelectricity with Long ion displacements in crystals of non - polar point groups. *Adv. Funct. Mater.* **34**:2404665. DOI:10.1002/adfm.202404665
10. Lu C., Wu M., Lin L., et al. (2019). Single-phase multiferroics: New materials, phenomena, and physics. *Natl. Sci. Rev.* **6**:653–668. DOI:10.1093/nsr/nwz091
11. Dong S., Xiang H. and Dagotto E. (2019). Magnetoelectricity in multiferroics: A theoretical perspective. *Natl. Sci. Rev.* **6**:629–641. DOI:10.1093/nsr/nwz023
12. Zhong T., Li X., Wu M., et al. (2020). Room-temperature multiferroicity and diversified magnetoelectric couplings in 2D materials. *Natl. Sci. Rev.* **7**:373–380. DOI:10.1093/nsr/nwz169
13. Sun Z., Su Y., Zhi A., et al. (2024). Evidence for multiferroicity in single-layer $CuCrSe_2$. *Nat. Commun.* **15**:4252. DOI:10.1038/s41467-024-48636-z
14. Wang P., Zhao Y., Na R., et al. (2024). Chemical vapor deposition synthesis of intrinsic high-temperature ferroelectric 2D $CuCrSe_2$. *Adv. Mater.* **36**:e2400655. DOI:10.1002/adma.202400655
15. Xu X., Zhong T., Zuo N., et al. (2022). High-T*c* two-dimensional ferroelectric $CuCrS_2$ grown via chemical vapor deposition. *ACS Nano* **16**:8141–8149. DOI:10.1021/acsnano.2c01470
16. Zhang Z., Xia J., Li J., et al. (2025). Robust ferroelectricity in nonstoichiometric 2D $AgCr_{1-x}S_2$ via chemical vapor deposition. *Small* **21**:e2409004. DOI:10.1002/smll.202409004
17. Xing J., Tang Y., Li J., et al. (2024). Intrinsic out-of-plane and in-plane ferroelectricity in 2D $AgCrS_2$ with high curie temperature. *Adv. Mater.* **36**:e2407655. DOI:10.1002/adma.202407655
18. Wu J., Zhu H., Li X., et al. (2025). Dynamics of ferroelectricity in monolayer $AgCr_2S_4$ calculated with a machine learning potential. *Phys. Rev. B* **111**:085417. DOI:10.1103/PhysRevB.111.085417
19. Zhao Y., Liu Q., Zhang F., et al. (2022). Multiferroicity in a two-dimensional non-van der Waals crystal of $AgCr_2X_4$ (X = S or Se). *J. Phys. Chem. Lett.* **13**:11346–11353. DOI:10.1021/acs.jpclett.2c03160
20. Wang Y. and Wu M. (2024). Facile coordination transitions in $AgCrX_2$ (X = S, Se): Unprecedented electrostrain, negative piezoelectricity and thermal expansion. *Nano Lett.* **24**:9868–9873. DOI:10.1021/acs.nanolett.4c02037
21. Du K., Guo L., Peng J., et al. (2020). Direct visualization of irreducible ferrielectricity in crystals. *npj Quantum Mater.* **5**:49. DOI:10.1038/s41535-020-00252-y
22. Sun W., Ye H., Liang L., et al. (2024). Stacking-dependent ferroicity of a reversed bilayer: Altermagnetism or ferroelectricity. *Phys. Rev. B* **110**:224418. DOI:10.1103/PhysRevB.110.224418
23. Sheng Y., Zhang J., Liu J., et al. (2025). Ubiquitous van der Waals altermagnetism with sliding/moire ferroelectricity. *Sci. China: Phys. Mech. Astron.* **68**:297511. DOI:10.1007/s11433-025-2698-5
24. Zhong T., Zhang H. and Wu M. (2024). Single molecular semi-sliding ferroelectricity/multiferroicity. *Research* **7**:0428. DOI:10.34133/research.0428
25. Yang Q., Zhong T., Tu Z., et al. (2019). Design of single-molecule multiferroics for efficient ultrahigh-density nonvolatile memories. *Adv. Sci.* **6**:1801572. DOI:10.1002/advs.201801572
26. Meng J., Su Y., Zhu H., et al. (2024). Shape memory and self-healing in a molecular crystal with inverse temperature symmetry breaking. *Chem. Sci.* **15**:5738–5745. DOI:10.1039/d3sc06800e
27. Zhan L. Y., Zhou Y., Li N., et al. (2024). A high working temperature multiferroic induced by inverse temperature symmetry breaking. *J. Am. Ceram. Soc.* **146**:5414–5422. DOI:10.1021/jacs.3c12842
28. Lei Y., Yang X., Wang S., et al. (2025). Electric field control of spin orbit coupling and circular photogalvanic effect in a true ferrielectric crystal. *Natl. Sci. Rev.* **12**:nwaf320. DOI:10.1093/nsr/nwaf320
29. Cococcioni M. and de Gironcoli S. (2005). Linear response approach to the calculation of the effective interaction parameters in the LDA+U method. *Phys. Rev. B* **71**:035105. DOI:10.1103/PhysRevB.71.035105
30. Dudarev S. L., Botton G. A., Savrasov S. Y., et al. (1998). Electron-energy-loss spectra and the structural stability of nickel oxide: An LSDA+U study. *Phys. Rev. B* **57**:1505–1509. DOI:10.1103/PhysRevB.57.1505
31. Perdew J. P., Burke K. and Ernzerhof M. (1996). Generalized gradient approximation made simple. *Phys Rev Lett* **77**:3865–3868. DOI:10.1103/PhysRevLett.77.3865
32. Blochl P. E. (1994). Projector augmented-wave method. *Phys. Rev. B* **50**:17953–17979. DOI:10.1103/physrevb.50.17953
33. Grimme S., Ehrlich S. and Goerigk L. (2011). Effect of the damping function in dispersion corrected density functional theory. *J. Comput. Chem.* **32**:1456–1465. DOI:10.1002/jcc.21759
34. Monkhorst H. J. and Pack J. D. (1976). Special points for Brillouin-zone integrations. *Phys. Rev. B* **13**:5188–5192. DOI:10.1103/PhysRevB.13.5188
35. Henkelman G., Uberuaga B. P. and Jónsson H. (2000). A climbing image nudged elastic band method for finding saddle points and minimum energy paths. *J. Phys. Chem. Lett.* **113**:9901–9904. DOI:10.1063/1.1329672
36. King-Smith R. D. and Vanderbilt D. (1993). Theory of polarization of crystalline solids. *Phys. Rev. B* **47**:1651–1654. DOI:10.1103/physrevb.47.1651
37. Zhang L., Han J., Wang H., et al. (2018). Deep potential molecular dynamics: A scalable model with the accuracy of quantum mechanics. *Phys Rev Lett* **120**:143001. DOI:10.1103/PhysRevLett.120.143001
38. Wang H., Zhang L., Han J., et al. (2018). DeePMD-kit: A deep learning package for many-body potential energy representation and molecular dynamics. *Comput. Phys. Commun.* **228**:178–184. DOI:10.1016/j.cpc.2018.03.016
39. Plimpton S. (1995). Fast parallel algorithms for short-range molecular dynamics. *J. Comput. Phys.* **117**:1–19. DOI:10.1006/jcph.1995.1039

FUNDING AND ACKNOWLEDGMENTS

This work was supported by the National Natural Science Foundation of China (12574263). The funder had no role in study design, data collection and analysis, decision to publish, or preparation of the manuscript.

AUTHOR CONTRIBUTIONS

Y. S. performed the calculations. M. W. designed and supervised the research. All authors contributed to the manuscript and approved the final version.

DECLARATION OF INTERESTS

The authors declare no competing interests.

DATA AND CODE AVAILABILITY

Data are available from the corresponding author upon reasonable request.

SUPPLEMENTAL INFORMATION

It can be found online at https://doi.org/10.59717/j.tip.2026.100017.